Apolipoprotein E4 causes age-dependent disruption of slow gamma oscillations during hippocampal sharp-wave ripples

Anna K. Gillespie[1,2], **Emily A. Jones**[1,2], **Yuan-Hung Lin**[1,3], **Mattias P. Karlsson**[4], **Kenneth Kay**[4,5], **Seo Yeon Yoon**[1], **Leslie M. Tong**[1,2], **Philip Nova**[1,2], **Jessie S. Carr**[1,6], **Loren M. Frank**[3,4,5], and **Yadong Huang**[1,2,6,7]

[1]Gladstone Institute of Neurological Disease, San Francisco, CA 94158, USA

[2]Biomedical Sciences Graduate Program, University of California, San Francisco, CA 94143, USA

[3]Neuroscience Graduate Program, University of California, San Francisco, CA 94143, USA

[4]Center for Integrative Neuroscience and Department of Physiology, University of California, San Francisco, CA 94158, USA

[5]Bioengineering Graduate Program, University of California, San Francisco, CA 94143, USA

[6]Pharmaceutical Sciences and Pharmacogenomics Graduate Program, University of California, San Francisco, CA 94143, USA

[7]Departments of Neurology and Pathology, University of California, San Francisco, CA 94143, USA

SUMMARY

Apolipoprotein (apo) E4 is the major genetic risk factor for Alzheimer's disease (AD), but the mechanism by which it causes cognitive decline is unclear. In knock-in (KI) mice, human apoE4 causes age-dependent learning and memory impairments and degeneration of GABAergic interneurons in the hippocampal dentate gyrus. Here we report two functional apoE4-KI phenotypes involving sharp-wave ripples (SWRs), hippocampal network events critical for memory processes. Aged apoE4-KI mice had fewer SWRs than apoE3-KI mice and significantly reduced slow gamma activity during SWRs. Elimination of apoE4 in GABAergic interneurons, which prevents learning and memory impairments, rescued SWR-associated slow gamma activity but not SWR abundance in aged mice. SWR abundance was reduced similarly in young and aged

apoE4-KI mice; however, the full SWR-associated slow gamma deficit emerged only in aged apoE4-KI mice. These results suggest that progressive decline of interneuron-enabled slow gamma activity during SWRs critically contributes to apoE4-mediated learning and memory impairments.

INTRODUCTION

As one of the most common diseases among aging populations, Alzheimer's disease (AD) progressively disrupts memory function, ultimately robbing patients of their independence, their sense of self, and their ability to recognize and interact with family and community. One of the earliest sites of AD pathology is the hippocampus, a brain structure critical for the learning and memory processes that falter early in AD. Decades of research have yielded insight into the genetics and cellular pathology of the disease, but it is unclear how these pathologies disrupt hippocampal memory processes.

The main genetic risk factor for AD is apolipoprotein (apo) E4 (Corder et al., 1993; Saunders et al., 1993; Strittmatter et al., 1993), one of three isoforms of the apoE protein in humans. Present in 65–80% of AD cases, apoE4 increases the incidence of AD and lowers the age of onset in a gene dose-dependent manner (Farrer et al., 1997) compared to the most common isoform, apoE3. This effect is gender-dependent; female apoE4 carriers are more likely to develop AD than male apoE4 carriers independent of longevity and disease mortality factors (Beydoun et al., 2012; Farrer et al., 1997). The mechanisms of apoE4 pathogenesis can be investigated in mice by replacing the endogenous apoE allele with the human apoE4 or apoE3 allele. These knock-in (KI) mice express human apoE isoforms at physiological levels in appropriate cell populations (Bien-Ly et al., 2012; Ramaswamy et al., 2005) and recapitulate the gender bias seen in humans (Leung et al., 2012). By 16 months of age, female apoE4-KI mice have robust learning and memory deficits, as shown by impaired performance in the Morris water maze (Andrews-Zwilling et al., 2010; Leung et al., 2012).

Further investigation revealed a cellular phenotype that precedes behavioral impairment. Beginning at 6 months of age, apoE4-KI mice show accelerated age-related loss of hilar GABAergic interneurons (predominantly somatostatin-positive), in the dentate gyrus (DG) of the hippocampus. Multiple lines of evidence link this interneuron loss to the observed behavioral deficits. First, the extent of loss predicts the severity of impairment (Andrews-Zwilling et al., 2010; Leung et al., 2012). Second, optogenetic silencing of GABAergic interneurons in the hilus recapitulates apoE4-induced learning and memory impairment (Andrews-Zwilling et al., 2012). Third, transplantation of GABAergic interneurons into the hilus restores normal learning and memory in aged apoE4-KI mice (Tong et al., 2014). Finally, selective elimination of apoE4 from GABAergic interneurons prevents learning and memory deficits and loss of hilar interneurons (Knoferle et al., 2014).

Importantly, although these cellular and behavioral phenotypes are well established, the circuit-level link between them is unclear. We therefore set out to understand how cellular pathology in apoE4-KI mice, including the loss of hilar GABAergic interneurons, drives alterations in hippocampal network activity and thus causes learning and memory deficits. We focused on hippocampal sharp-wave ripple (SWR) network events, as they have been

causally linked to memory processes (Ego-Stengel and Wilson, 2010; Girardeau et al., 2009; Jadhav et al., 2012).

SWRs are characterized by short bursts of a high-frequency oscillation (ripple band, 150–250 Hz) in the local field potential (LFP) recorded from the CA1 region during periods of awake immobility and slow-wave sleep (Buzsaki et al., 2003; Buzsaki et al., 1992). This oscillation marks the firing of pyramidal cell ensembles that can encode past experiences, such that their activation comprises a time-compressed "replay" of that experience (Buzsaki, 2015; Lee and Wilson, 2002; Skaggs and McNaughton, 1996). The disruption of SWRs causes memory impairment (Ego-Stengel and Wilson, 2010; Girardeau et al., 2009; Jadhav et al., 2012), consistent with a critical role in memory consolidation and possibly retrieval (Buzsaki, 1989, 1996; Kudrimoti et al., 1999). SWRs have also been implicated in memory processing in humans (Clemens et al., 2007; Le Van Quyen et al., 2008), but our understanding of their role in neurodegenerative disease is limited (Ciupek et al., 2015; Witton et al., 2014).

During SWRs, a 20–50 Hz oscillation called hippocampal slow gamma entrains activity across CA3 and CA1. Higher coherence and phase locking of slow gamma between CA3 and CA1 during individual SWRs predicts higher-fidelity memory replay (Carr et al., 2012). As replay events involve sequential activity of cells distributed across CA3 and CA1 regions of both hemispheres, the slow gamma rhythm is thought to promote the coordination of hippocampal neural ensembles across regions and hemispheres necessary to produce accurate replay (Carr et al., 2012; Colgin, 2012). More recently, the progression of spatial locations represented by firing during replay was found to advance in discrete segments, in a manner time-locked to the slow gamma oscillation (Pfeiffer and Foster, 2015). Together, these findings suggest a critical role for slow gamma oscillations during SWRs in organizing coherent replay events.

In this study, we found that apoE4-KI mice have reduced abundance of SWRs regardless of age, and attenuated transient slow gamma oscillations during SWRs, dependent on aging. Eliminating apoE4 from GABAergic interneurons rescued the slow gamma activity associated with SWRs, but not SWR abundance. Since GABAergic interneuron-specific elimination of apoE4 has been shown to prevent learning and memory impairment (Knoferle et al., 2014), these findings suggest that interneuron-mediated deficits in SWR-associated slow gamma activity contribute to apoE4-induced learning and memory impairments.

RESULTS

To identify the hippocampal network phenotype in a mouse model of AD, we recorded hippocampal neural activity in female apoE3-KI ($n = 14$) and apoE4-KI ($n = 13$) mice aged 12–18 months. We chose apoE3-KI mice as the most appropriate control because they are phenotypically indistinguishable from wild-type mice, even though human apoE3 differs from mouse apoE in some aspects (Huang and Mucke, 2012). Using apoE3-KI mice also allows us to relate our findings to previous studies of these genotypes. Chronic 32-channel silicon arrays were targeted to distribute recording sites across the CA1, CA3, and DG subregions of the hippocampus (Figure 1A). Recording sites were assigned specific layer

locations based on histology (Figure 1B) and LFP characteristics (Figure 1C). Data were collected over several long sessions in the home cage, during which the mice behaved freely, often resting or sleeping. To increase hippocampal engagement, mice were exposed to several novel environments interspersed with rest sessions in the home cage (Karlsson and Frank, 2008). Since SWRs are most abundant during sleep or quiet wakefulness (Buzsaki et al., 1992), we focused on LFP data during periods of immobility lasting 30 s or more (rest state). The recording site closest to the center of the CA1 pyramidal cell layer in each mouse was used to detect SWRs, defined by a ripple-filtered LFP trace exceeding several standard deviations (SD) above baseline (see Methods).

SWR abundance is reduced in aged apoE4-KI mice

SWRs in aged apoE3-KI and apoE4-KI mice appeared qualitatively similar in the raw and ripple-filtered LFP traces (Figure 2A). However, across a range of detection thresholds, SWRs were substantially less abundant in apoE4-KI mice during rest (Figure 2B). To ensure that this reduction did not reflect differences in event detection in the two genotypes, we verified that the measures for SWR detection (baseline and SD of the ripple-filtered signal) were not different (Figure S1A and S1B), confirming that the events detected for each genotype were comparable.

Analysis of power spectra during SWRs showed that the frequency range of ripple oscillations was lower in aged apoE4-KI mice than in apoE3-KI mice (Figure 2C), and peak ripple power occurred at a lower frequency (156.7 ± 1.6 Hz vs 173.1 ± 5.5 Hz; Figure 2D). As this placed the predominant frequency of SWR oscillations in the apoE4-KI mice close to the boundary of our defined ripple band (150–250 Hz), we wondered whether the reduction of SWRs in apoE4-KI mice could result from our definition of the ripple frequency band. To address this concern, we expanded the ripple frequency range for SWR detection to 125–250 Hz. Detected SWRs increased in both genotype groups, but SWR abundance remained lower in apoE4-KI mice than apoE3-KI mice (Figure S1D). The frequency of peak ripple power in apoE4-KI mice also remained similar despite the wider ripple frequency range (153.5 ± 4.8 Hz vs 173.3 ± 6.7 Hz; Figure S1E). Thus, apoE4-induced reduction of SWR abundance reflects a lack of events rather than a failure to detect them. For subsequent analyses, the 150–250 Hz ripple band was used.

ApoE4-induced reduction in SWR abundance could be due to a failure in event generation or to a consistent reduction of SWR amplitude below the detection threshold. However, the distribution of SWR sizes (Figure 2E) and the average SWR size (Figure 2E, inset) were similar in the two groups, suggesting that aged apoE4-KI mice generate fewer SWRs than apoE3-KI mice. In addition, the average length of SWRs was greater in the apoE4-KI mice (Figure S1C), which could be a compensatory effect or might indicate further dysregulation of SWRs in apoE4-KI mice.

To determine whether SWR regulation was generally impaired in aged apoE4-KI mice, we took advantage of the increase in SWR abundance after exposure to a novel environment (Karlsson and Frank, 2008; Larkin et al., 2014; O'Neill et al., 2008). In both genotypes, SWRs were more frequent during rest in the home cage immediately after exposure to a novel environment than at baseline (Figure 2F). Genotype and environment had significant

effects but did not interact, as shown by two-way ANOVA. Accordingly, the percentage increase did not differ between genotypes. Thus, the ability to generate SWRs was impaired in aged apoE4-KI mice, but the mechanism of novelty-driven increase in SWRs was intact.

Slow gamma power increases in the DG during SWRs in mice

We next asked whether the slow gamma oscillations seen during SWRs in rats (Carr et al., 2012; Pfeiffer and Foster, 2015) are also present in mice. In the phenotypically normal apoE3-KI mice, SWR-triggered spectrograms showed a distinct peak in the slow gamma range (20–50 Hz) (Figure 3A), suggesting that the slow gamma band occupies similar frequencies in mice and rats. As in rats, this SWR-associated slow gamma power was present in the CA1 pyramidal cell layer, highest in the CA1 stratum radiatum, and also present in the CA3 pyramidal cell layer and CA3 stratum radiatum. As expected, low-frequency power (< 20 Hz) also increased transiently during SWRs, likely reflecting the sharp-wave component of the SWRs (Buzsaki, 1986).

Importantly, slow gamma activity in the DG increased during SWRs (Figure 3A, bottom) in every apoE3-KI mouse, indicating that increased DG slow gamma activity is a common property of SWRs in these mice (Figure 3B). This finding was surprising because although some SWR-associated activity has been observed in the DG (Penttonen et al., 1997; Sullivan et al., 2011), and slow gamma outside of SWRs has been seen in the DG (Bragin et al., 1995a; Montgomery and Buzsaki, 2007), slow gamma activity in the DG time-locked to SWRs has not been reported. Given the challenge of accurately locating sites in the DG, we used the presence of dentate spikes (Bragin et al., 1995b; Penttonen et al., 1997) to validate hilar and granule cell layer channels, and it was in these locations that we observed the most slow gamma activity in the DG. To estimate the frequency of slow gamma oscillation during SWRs, we filtered the raw signal between 15 and 50 Hz and converted the distance between each peak of the filtered oscillation to a measure of instantaneous frequency (Carr et al., 2012). In all subregions, there was a single peak in the distribution of samples at approximately 42 Hz (Figure 3C), suggestive of a single slow gamma oscillation in all three subregions during SWRs.

To eliminate the possibility that this signal simply resulted from volume conduction, we examined the slow gamma signal across the DG and surrounding sites. The power varied substantially between sites and there was little commonality between neighboring channels (Figure S2). In the majority of cases, maximal slow gamma power was higher in the granule cell layer or hilus than in surrounding sites. Current source density (CSD) analysis in several animals that received probes with 100-μm spacing between electrode sites (Figure 3D) showed distinct regions of slow gamma activity in the DG that were separated from CA1, confirming that the observed slow gamma activity could not be due to volume conduction (Figure 3E).

The coherence of slow gamma between CA3 and CA1 indicates coordination between the two regions, enabling organized, accurate replay (Carr et al., 2012). Indeed, when we calculated the coherence between CA1 stratum radiatum and the other subregions, we found a distinct, specific increase in the coherence of slow gamma during SWRs throughout the circuit. In particular, this was evident between DG hilus and CA1 stratum radiatum in all

mice (Figure 3F and G), further indicating the involvement of the DG with the rest of the hippocampal circuit during SWRs. Slow gamma coherence between CA3 and CA1 stratum radiatum was also increased during SWRs (Figure 3H and 3I), as in rats (Carr et al., 2012).

The SWR-associated slow gamma power in the DG and the transient increase in slow gamma coherence between the DG and CA1 during SWRs strongly suggest that in addition to CA3-CA1 coordination during SWRs, the DG may also be critically involved. These three subregions participate in a common, coherent slow gamma oscillation likely involved in coordinating hippocampal replay.

Slow gamma power during SWRs is reduced in aged apoE4-KI mice

Next, we investigated whether slow gamma during SWRs is affected in aged apoE4-KI mice. We found that SWR-associated slow gamma power was significantly lower in aged apoE4-KI mice than in apoE3-KI mice (Figure 4A and 4B). The reduction was most prominent in the CA1 stratum radiatum, averaging nearly 50% lower than in apoE3-KI mice, and was significant in the CA3 and DG as well (Figure 4D).

Although overall slow gamma activity was lower, we still saw significant variability among neighboring channels and no evidence of volume conduction of slow gamma activity in apoE4-KI mice (Figure S3). The average instantaneous frequency of slow gamma activity did not differ across genotypes (Figure 4C). Outside of SWRs, the baseline and standard deviation of slow gamma filtered activity did not differ between genotype groups (Figure S4A), indicating that the apoE4-KI mice are generally capable of sustaining slow gamma oscillations. These observations suggest that the mechanism for generating slow gamma oscillations is intact in aged apoE4-KI mice, but the engagement of slow gamma during SWRs is compromised.

To characterize the reduction of SWR-associated slow gamma power at the level of individual SWRs, we quantified the distribution of slow gamma power over all SWRs for each mouse and averaged by genotype (Figure 4E). ApoE4-KI mice had many more SWRs in which slow gamma power decreased or did not increase, and in those in which it did increase, the increase was smaller than in apoE3-KI mice—further evidence of disrupted slow gamma engagement during SWRs in aged apoE4-KI mice.

We assessed the coherence of SWR-associated slow gamma activity between hippocampal subregions in a subset of aged apoE4-KI and apoE3-KI SWRs with similar slow gamma power. With respect to CA1 stratum radiatum coherence with DG hilus and CA3, the genotypes did not differ before SWRs (baseline), during the peak of SWRs, or in the increase from baseline to peak (Figure S4B and S4C). Evidently, although slow gamma engagement may be impaired overall, coordination between hippocampal subregions is maintained in aged apoE4-KI mice.

Removing apoE4 from GABAergic interneurons rescues slow gamma power but not SWR abundance in aged mice

We next explored whether these circuit-level findings were related to cognitive impairment and GABAergic interneuron loss. Previously, we showed that removing pathogenic apoE4

only in GABAergic interneurons prevents learning and memory impairments in aged apoE4-KI mice (Knoferle et al., 2014). We took advantage of this finding to determine whether the network activity alterations described contribute to apoE4-induced behavioral deficits. We crossed KI mice expressing a floxed human apoE4 allele with mice expressing Cre recombinase under the control of the forebrain GABAergic interneuron-specific enhancer, Dlx-I12b (Potter et al., 2009). The resulting apoE4-KI/Dlx-Cre mice express apoE4 in all cells except forebrain GABAergic interneurons. These mice do not show hilar GABAergic interneuron degeneration or learning and memory impairment, even at advanced age (Knoferle et al., 2014). Thus, we hypothesized that GABAergic interneuron-specific deletion of apoE4 would rescue abnormalities in neural activity critical for learning and memory.

Recordings from aged female apoE4-KI/Dlx-Cre mice ($n = 8$) showed reduced SWR abundance but restored SWR-associated slow gamma activity. During rest in the home cage, SWR abundance was significantly lower in aged apoE4-KI/Dlx-Cre mice than in apoE3-KI mice and nearly identical to that of aged apoE4-KI mice across a range of detection thresholds (Figure 5A). The baseline and standard deviation for SWR detection did not differ significantly across the three genotype groups, and nor did the average SWR size or the distribution of SWR sizes (Figure S5A, S5C, and S5D). The reduction of predominant ripple frequency (Figure S5B) and increase in SWR length (Figure S5E) were similar for apoE4-KI and apoE4-KI/Dlx-Cre mice compared to apoE3-KI mice. The lack of rescue of these intrinsic SWR characteristics and SWR generation indicates that apoE4's effects are not restricted to GABAergic interneurons.

In contrast, the power of slow gamma activity during SWRs was completely rescued in all three subregions of the hippocampus in aged apoE4-KI/Dlx-Cre mice (Figure 5B and 5D). The distribution of slow gamma power across SWRs was nearly identical in aged apoE4-KI/Dlx-Cre and aged apoE3-KI mice (Figure 5E). The instantaneous frequency of slow gamma and measures of slow gamma coherence in the apoE4-KI/Dlx-Cre group were similar to those in the apoE3-KI and apoE4-KI groups (Figure 5C and Figure S5F and S5G). Thus, the disruption of SWR-associated slow gamma activity in aged apoE4-KI mice was specifically and robustly rescued in aged apoE4-KI/Dlx-Cre mice. This result suggests that intact GABAergic interneurons enable normal levels of SWR-associated slow gamma activity. Since aged apoE4-KI/Dlx-Cre mice show no impairment in learning or memory (Knoferle et al., 2014), this finding further implicates disrupted slow gamma activity during SWRs as a circuit-level mechanism of apoE4-induced cognitive impairment.

SWR abundance and SWR-associated slow gamma activity in apoE4-KI mice are differentially affected by aging

To extend our understanding of the interplay between interneuron loss, hippocampal network activity alteration, and behavioral impairment, we assessed the electrophysiological phenotypes of female apoE3-KI ($n = 9$) and apoE4-KI ($n = 7$) mice at 4–5 months of age, before apoE4-induced interneuron loss is significant and when learning and memory deficits are undetectable (Andrews-Zwilling et al., 2010; Leung et al., 2012). Strikingly, compared to young apoE3-KI mice, the young apoE4-KI mice already had a significant reduction in SWR abundance (Figure 6A), lower intrinsic SWR frequency (Figure 6B), and increased

SWR length (Figure 6C), similar to the effects seen in the aged groups. The baseline and standard deviation of ripple power were similar in young apoE3-KI and apoE4-KI mice (Figure S6A and S6B). Thus, apoE4-KI network alterations relating to SWR generation and activity in the ripple frequency band are present in young apoE4-KI mice long before behavioral impairment is detectable. Although these changes may interact with other factors to contribute to impairment with advanced age, they are not likely to directly initiate learning and memory deficits.

In contrast, the SWR-associated slow gamma phenotype in young apoE4-KI mice was distinct from that of aged apoE4-KI mice. The instantaneous frequency of slow gamma activity during SWRs did not differ in the young genotype groups (Figure S6C) and was similar to that in aged mice. Unlike the attenuation in aged apoE4-KI mice, SWR-associated slow gamma activity was not significantly reduced in CA3 or the DG, although it was in CA1 stratum radiatum (Figure 6D). The source of this attenuation differed from that of aged apoE4-KI mice; however, the distribution of slow gamma power in CA1 stratum radiatum across SWRs revealed that the difference was driven primarily by reduction of the proportion of SWRs with exceptionally high slow gamma power (Figure 6E). Truncating the distribution at 7 SD above the mean (z-score value of 7) eliminated the difference in mean values (Figure 6E, inset), despite eliminating relatively few SWRs ($6.9 \pm 0.7\%$ for young apoE3-KI mice and $2.4 \pm 0.5\%$ for young apoE4-KI mice). Further, the distribution of CA1 stratum radiatum SWR-associated slow gamma power for young apoE4-KI mice was far more similar to apoE3-KI mice of both ages than to aged apoE4-KI mice (Figure 6F). In contrast to the young mice, truncation of the distribution at a z-scored slow gamma power value of 7 did not eliminate the differences between aged apoE4-KI mice and aged apoE3-KI mice (Figure 6G). This underscores that in the aged apoE4-KI mice, the majority of SWRs show attenuated slow gamma activity, while in the young apoE4-KI mice, excluding a small minority of SWRs abolishes the reduction in CA1 stratum radiatum slow gamma activity. Additionally, the fraction of SWRs with suppression of CA1 stratum radiatum slow gamma below baseline was significantly greater in aged apoE4-KI mice than in any other group (Figure 6H).

These findings, coupled with the lack of significant reduction in SWR-associated slow gamma power in CA3 and the DG, suggest that the SWR-associated slow gamma deficit depends on both apoE genotype and age. This age-related progression, together with the rescue of both SWR-associated slow gamma and cognitive impairment by removal of apoE4 from GABAergic interneurons, support the idea that dysregulation of SWR-associated slow gamma power critically contributes to apoE4-induced, age-related impairments in learning and memory.

DISCUSSION

To identify hippocampal network signatures of apoE4-induced memory malfunction, we compared network activity in multiple hippocampal subregions of apoE3-KI and apoE4-KI mice. We focused on SWRs, which have been linked to memory consolidation and retrieval. We found that in contrast to age-matched apoE3-KI mice, aged apoE4-KI mice showed substantial reduction of SWR-associated slow gamma activity in all hippocampal

subregions. Furthermore, in aged apoE4-KI/Dlx-Cre mice, which lack pathogenic apoE4 exclusively in forebrain GABAergic interneurons, slow gamma activity during SWRs was preserved throughout the hippocampal circuit. Since aged apoE4-KI/Dlx-Cre mice do not have hilar interneuron loss or learning and memory deficits (Knoferle et al., 2014), these results implicate GABAergic interneuron-dependent SWR-associated slow gamma activity as a key factor in apoE4-induced learning and memory impairment (Figure 7). In support of this conclusion, young apoE4-KI mice had a distinct and less severe SWR-associated slow gamma phenotype, suggestive of an age-dependent progression of the slow gamma deficit coincident with interneuron loss. In addition, apoE4-KI mice irrespective of age showed reduced SWR abundance and altered intrinsic features of SWRs compared to apoE3-KI mice. In contrast to SWR-associated slow gamma activity, these abnormalities were not rescued by removal of apoE4 from GABAergic interneurons.

During SWRs, we found transient slow gamma oscillations in the CA1 and CA3 hippocampal subregions in mice, as reported in rats (Carr et al., 2012), and in the DG. We observed increased SWR-associated slow gamma coherence between CA3 and CA1 as previously established (Carr et al., 2012), and showed that the slow gamma in the DG became more coherent with CA1 slow gamma during SWRs. Thus, a single slow gamma oscillation engages the entire hippocampal circuit during SWRs, raising questions about information flow through the hippocampus during SWRs. CA3 has been implicated as a generator of slow gamma oscillations (Carr et al., 2012; Colgin et al., 2009; Csicsvari et al., 2003) and as the major excitatory drive to CA1 during SWRs (Bragin et al., 1995a; Csicsvari et al., 2000; Nakashiba et al., 2009; Ylinen et al., 1995). During SWRs, CA3 could entrain DG activity via the CA3 back-projection onto hilar mossy cells and interneurons (Myers and Scharfman, 2011; Scharfman, 2007). In this way, CA3 synaptic activity could promote synchronous slow gamma activity in both subregions, through the back-projection to DG and simultaneously through recurrent collaterals in CA3.

While CA3 may be a main driver of SWR-associated slow gamma activity, our results suggest that interneuron populations, particularly those in the DG, have an essential role in supporting or regulating slow gamma activity. Eliminating apoE4 in interneurons abolishes apoE4-induced learning and memory impairments (Knoferle et al., 2014). We found that it also prevents apoE4-induced SWR-associated slow gamma impairment. ApoE4-KI mice have loss of GABAergic interneurons in the hilus of the DG and no evident cellular degeneration in CA3, CA1, or entorhinal cortex at the ages analyzed (Andrews-Zwilling et al., 2010; Leung et al., 2012). There is substantial evidence that interneuron populations are critical for supporting gamma oscillations (Mann and Paulsen, 2005), and our apoE4-KI/ Dlx-Cre results suggest that interneurons, particularly in the DG, might be important for SWR-associated slow gamma activity throughout the hippocampal circuit.

The distinct SWR-associated slow gamma phenotype in young apoE4-KI mice also supports this model. In apoE4-KI mice, interneuron loss is not evident at 3 months of age, becomes significant at 6 months, and progresses with age. Thus, the 4–5-month-old apoE4-KI mice we used likely have minimal interneuron loss compared to age-matched apoE3-KI mice. Accordingly, SWR-associated slow gamma power in the DG or CA3 was not significantly reduced in the young mice. However, we did see a trend toward lower slow gamma power

during SWRs in these regions in young apoE4-KI mice, potentially reflecting early interneuron loss in some mice. Interestingly, SWR-associated slow gamma power in the CA1 stratum radiatum was significantly attenuated in the young apoE4-KI mice, although to a lesser extent than in aged apoE4-KI mice. This raises the possibility that despite the absence of overt cellular loss at this age, a subset of CA1 interneurons might already be functionally affected in young mice. However, the distribution of slow gamma power over SWRs was relatively similar in young apoE3-KI and apoE4-KI mice, with a small fraction of SWRs in the tail of the distribution accounting for the decrease in mean CA1 stratum radiatum power. In contrast, the majority of SWRs shows low or decreased slow gamma power in aged apoE4-KI mice compared to all other groups. Additionally, the fraction of SWRs with suppressed slow gamma activity below baseline was significantly less in young than in aged apoE4-KI mice, further evidence of an age-dependent progressive phenotype. Together, these findings reveal an age-dependent decline of slow gamma activity during SWRs in apoE4-KI mice. The progression of this phenotype likely reflects age-dependent interneuron loss and may ultimately contribute to learning and memory impairments.

Strikingly, the removal of apoE4 from interneurons did not rescue the abundance of SWRs in apoE4-KI/Dlx-Cre mice, and the abundance was also substantially reduced even in young apoE4-KI mice. Similarly, both young and aged apoE4-KI mice had a lower intrinsic ripple frequency and longer SWRs, neither of which was rescued in the apoE4-KI/Dlx-Cre mice. Thus, apoE4-induced pathology in other cell populations (excitatory neurons or non-neuronal cell types) impairs these characteristics and is an early, or even developmental, effect of apoE4 expression. Although the early SWR generation and ripple oscillation-related abnormalities may interact with other factors to contribute to impairment with advanced age, their lack of progression suggests that they are unlikely to directly initiate learning and memory impairment.

Because aged apoE4-KI/Dlx-Cre mice have unimpaired learning and memory (Knoferle et al., 2014), our findings suggest that normal slow gamma activity during SWRs is sufficient for intact learning and memory even when SWR abundance is reduced. Young apoE4-KI mice also have no cognitive impairments (Andrews-Zwilling et al., 2010; Leung et al., 2012), despite reduced SWR abundance and the limited alteration of SWR-associated slow gamma activity. This suggests that SWR-associated slow gamma activity above a certain threshold enables normal learning and memory processes. Interestingly, SWR abundance is reduced in rTg4510 mice, a model of tauopathy related to many dementias, including AD. Surprisingly, despite having more severe cellular degeneration and behavioral impairments (Ramsden et al., 2005; Santacruz et al., 2005), rTg4510 mice have an SWR abundance similar to that of apoE4-KI mice (Ciupek et al., 2015; Witton et al., 2014). Thus, changes in SWR abundance might not be sufficient to explain the behavioral phenotype. SWR-associated slow gamma activity remains to be examined in this model.

The dissociation between the rescued SWR-associated slow gamma activity and the unchanged SWR abundance deficit in apoE4-KI/Dlx-Cre mice, together with the differential phenotype seen in the young apoE4-KI mice, raises questions about the regulation of these two oscillations. The mechanism that couples slow gamma activity to SWRs is unknown. Since apoE4-KI mice show normal slow gamma baseline power and standard deviation, this

suggests a problem with regulation of slow gamma activity during SWRs rather than an inability to generate the oscillation. Slow gamma oscillations during SWRs organize sequential spiking activity across hippocampal into trajectories representing past or potential future experience (Carr et al., 2012; Pfeiffer and Foster, 2013, 2015). Therefore, perhaps SWRs lacking slow gamma activity maintain overall firing rates but lack the temporal coordination necessary for proper memory function. In contrast, even if fewer SWRs occur, as in young apoE4-KI and aged apoE4-KI/Dlx-Cre mice, intact slow gamma activity during the majority of the remaining SWRs may be sufficient to sustain adequate memory processing.

Our findings show that SWR-associated slow gamma activity is substantially and specifically dysregulated in aged apoE4-KI mice and thus suggest a circuit-level mechanism of cognitive impairment in AD. Given the role of SWR-associated slow gamma activity in coordinating sequential replay in the hippocampus, the age-dependent SWR-associated slow gamma deficit in apoE4-KI mice is likely to contribute to their learning and memory impairments. Although it has not been assessed specifically during SWRs, hippocampal gamma activity has been linked to memory processing in humans (Lega et al., 2016; Sederberg et al., 2007), supporting the idea that apoE4-induced slow gamma disruption might contribute to learning and memory impairments in AD patients. Consistent with previous studies (Andrews-Zwilling et al., 2010; Knoferle et al., 2014; Leung et al., 2012), our findings implicate hilar GABAergic interneurons as a key target for therapeutic intervention in AD and promote the strengthening of hippocampal slow gamma coordination during SWRs as a candidate mechanism for cognitive protection.

EXPERIMENTAL PROCEDURES

Mice

Human apoE3-KI and apoE4-KI mice (Sullivan et al., 2004, RRID:MGI_MGI:2157240, RRID:MGI_MGI:2158398) were originally purchased from Taconic. LoxP-flanked apoE4-KI mice (Bien-Ly et al., 2012, RRID:MGI_MGI:5427463) were crossbred with Dlx-Cre transgenic mice [Tg(I12b-cre)] (Potter et al., 2009, RRID:MGI_MGI:3833422) to generate mice that were homozygous for apoE4 and positive for Dlx-Cre (apoE4-KI/Dlx-Cre) (Knoferle et al., 2014). All mice were maintained on a C57BL/6 background. Studies were conducted on female apoE3-KI, apoE4-KI, and apoE4-KI/Dlx-Cre mice at 12–18 months of age and apoE3-KI and apoE4-KI mice at 4–5 months of age. All mice were singly housed for the duration of the experiment on a 12-h light/12-h dark cycle and were not used for any other studies. Researchers were not blinded to animal genotype during experiments. All animal experiments were conducted in accordance with the guidelines of the National Institutes of Health, the University of California, and Gladstone Institutes.

Surgery

Mice were anesthetized by intraperitoneal injection of ketamine (60 mg/kg) and xylazine (30 mg/kg); anesthesia was maintained with 0.8–1% isofluorane given through a nose cone mounted on a stereotaxic alignment system (Kopf Instruments). The scalp was opened and sterilized with 3% hydrogen peroxide, and craniotomies were made over the right frontal

cortex and over the left parietal cortex. Skull screws (FST) were inserted to anchor and support the implant and were secured with dental adhesive (C&B Metabond, Parkell). An additional craniotomy was made over the cerebellum for insertion of the indifferent ground and reference wires. A fourth craniotomy was made centered at −1.95 mm AP and 1.5 mm ML from the bregma and extended bidirectionally along the ML axis until it was wide enough to accept the silicon probe. The probe was slowly lowered until the tip reached 2.2 mm beneath the surface of the brain, and the reference wire was inserted into the subdural space over the cerebellum. The probe was cemented in place with dental acrylic and the scalp was closed with sutures. The mice were treated with 0.0375 mg/kg buprenorphine intraperitoneally and 5 mg/kg ketofen subcutaneously 30–60 min after surgery and checked 24 h later. A minimum of 1 wk for recovery was allowed before recording. Probes were from NeuroNexus and for most mice had four 5-mm long shanks spaced 400 μm apart with 8 electrode sites per shank and 200 μm spacing between sites (configuration A4x8-400-200-704-CM32). Two apoE3-KI and one apoE4-KI mice had two-shank probes spaced 1600 μm apart with 16 sites per shank and 100 μm site spacing (configuration A2x16-1600-100-704-CM32). In these three mice, the reference electrode was placed over the frontal cortex instead of the cerebellum, but neither the probe configuration nor the reference placement significantly altered the results described.

Electrophysiology

Data from apoE3-KI, apoE4-KI, and apoE4-KI/Dlx-Cre mice were collected, amplified, processed, and digitized with a 32-channel Multichannel Acquisition Processor (Plexon) and a multiplexing headstage (Triangle Biosystems). Data were downsampled to 1000 Hz and bandpass filtered such that activity between 0.7 and 300 Hz was analyzed as LFP. Before data acquisition, all mice were allowed to habituate to the recording headstage and environment for 3 days (30–60 min/day in the home cage). The recording routine consisted of 5 days of home cage sessions (45–90 min/day) and then, for aged apoE3-KI and apoE4-KI groups, 3–5 days of novelty exposure (two 10-min sessions in a variety of novel environments separated by 10-min rest sessions in the home cage) (Karlsson and Frank, 2008). All sessions were completed during the day (light cycle). Video tracking was performed during all recording sessions with Ethovision (Noldus), which provided position information at 30 frames/sec.

Histology

Mice were deeply anesthetized with avertin, and a 30-μA current was passed through each recording site for 2 s to generate small electrolytic lesions. Each mouse was then perfused first with 10 ml of 0.9% NaCl and then with 10 ml of 4% paraformaldehyde; the brains were removed, further fixed in 4% PFA, cryoprotected in 30% sucrose, and stored at −20°C. Hemibrains were cut into 30-μm coronal sections with a microtome (Leica SM200R). Right hemibrains (containing the electrolytic lesions) were divided into subseries of every third section and used for Nissl staining to identify recording sites. Stained sections were examined with a Leica microscope.

Analysis of neural data

Neural data were analyzed with custom software written in MATLAB (Mathworks) with the Chronux toolbox (http://chronux.org) and the Plexon MAP offline software development kit (Plexon). The anatomical location of each electrode site was determined by examining Nissl-stained histological sections, raw LFP traces, the SWR-triggered spectrogram signature, and dentate spikes from each mouse. The raw LFP data were band-pass filtered at 150–250 Hz to detect SWRs and at 30–50 Hz to analyze slow gamma. A single channel in the CA1 pyramidal cell layer was used for ripple detection; SWRs were identified as times when the smoothed envelope of ripple-filtered data exceeded a certain threshold above baseline for at least 15 ms (Cheng and Frank, 2008). For most analyses, 5 SD was used as threshold unless otherwise specified (as in Figure 2B and 5A). The entire SWR was defined from the time of baseline crossing prior to threshold crossing until the envelope no longer exceeded the baseline value (Cheng and Frank, 2008).

Analysis of SWRs was restricted to periods of extended immobility, when mouse velocity was <1 cm/s for 30 s or more. For all ripple events, SWR-triggered spectrograms were calculated with the multitaper method, as described (Carr et al., 2012). For each channel, each ~7 Hz frequency band was z-scored according to the mean and SD of the power calculated across all immobile time within the behavioral epoch. For illustration in figures, spectrograms were computed with a 100-ms sliding window, in 10-ms steps; for quantification, a nonoverlapping 100-ms window was used. Quantification of slow gamma power reflects the average z-scored power over a 30–50-Hz frequency band at 1–100 ms after ripple detection, averaged over SWRs. Instantaneous frequency was calculated by filtering the raw signal with a 15–50-Hz filter, applying the Hilbert transform, and taking the reciprocal of the time between peaks (Carr et al., 2012).

Coherence was calculated with a multitaper time-frequency method (Chronux) that uses a 10-ms sliding window for visualization and a nonoverlapping 100-ms window for quantification. Coherence for all channels was calculated in relation to a single channel in CA1 stratum radiatum; coherence scores for channels in the same anatomical layer were averaged. For comparison between genotype groups, only SWRs with slow gamma in the 1–2 z-scored power range were included so that the power of slow gamma activity did not differ across groups, however, the results were not different if all SWRs were analyzed. Baseline coherence was quantified as the average coherence score over the 30–50-Hz frequency band 400–300 ms before SWR detection, peak coherence was calculated 0–100 ms after SWR detection, and the SWR-induced coherence increase was the difference between baseline and peak coherence.

For both power and coherence quantification, CA1-sr indicates measurements from the CA1 stratum radiatum channel most centrally located in the layer, CA3 indicates an average of sites in stratum pyramidale and radiatum, and DG indicates an average of sites in the hilus and granule cell layer (validated by the presence and polarity of dentate spikes). In mice with site spacing close enough to allow CSD analysis (100 μm), CSD was calculated as the second spatial derivative of the slow gamma-filtered (30–50 Hz) LFP signal (Bragin et al., 1995a).

Statistical analysis

All measurements from each mouse were averaged; thus, each mouse contributed a single number to the final comparison of genotypes. While conservative, this method avoids overrepresentation of any individual mouse and reduces the likelihood of artificially inflating significance based on large numbers of events. All data were normally distributed as shown by Lilliefors test, and variances between groups were similar as shown by Bartlett's test. For these reasons, we used two-tailed paired and unpaired *t* tests and one- and two-way ANOVA. Post hoc testing was done with Holm-Sidak correction for multiple comparisons.

Supplementary Material

Refer to Web version on PubMed Central for supplementary material.

Acknowledgments

References

Andrews-Zwilling Y, Bien-Ly N, Xu Q, Li G, Bernardo A, Yoon SY, Zwilling D, Yan TX, Chen L, Huang Y. Apolipoprotein E4 causes age- and Tau-dependent impairment of GABAergic interneurons, leading to learning and memory deficits in mice. J Neurosci. 2010; 30:13707–13717. [PubMed: 20943911]

Andrews-Zwilling Y, Gillespie AK, Kravitz AV, Nelson AB, Devidze N, Lo I, Yoon SY, Bien-Ly N, Ring K, Zwilling D, Potter GB, Rubenstein JL, Kreitzer AC, Huang Y. Hilar GABAergic interneuron activity controls spatial learning and memory retrieval. PLoS ONE. 2012; 7:e40555. [PubMed: 22792368]

Beydoun MA, Boueiz A, Abougergi MS, Kitner-Triolo MH, Beydoun HA, Resnick SM, O'Brien R, Zonderman AB. Sex differences in the association of the apolipoprotein E epsilon 4 allele with incidence of dementia, cognitive impairment, and decline. Neurobiol Aging. 2012; 33:720–731. e724. [PubMed: 20619505]

Bien-Ly N, Gillespie AK, Walker D, Yoon SY, Huang Y. Reducing human apolipoprotein E levels attenuates age-dependent Abeta accumulation in mutant human amyloid precursor protein transgenic mice. J Neurosci. 2012; 32:4803–4811. [PubMed: 22492035]

Bragin A, Jando G, Nadasdy Z, Hetke J, Wise K, Buzsaki G. Gamma (40–100 Hz) oscillation in the hippocampus of the behaving rat. J Neurosci. 1995a; 15:47–60. [PubMed: 7823151]

Bragin A, Jando G, Nadasdy Z, van Landeghem M, Buzsaki G. Dentate EEG spikes and associated interneuronal population bursts in the hippocampal hilar region of the rat. J Neurophysiol. 1995b; 73:1691–1605. [PubMed: 7643175]

Buzsaki G. Hippocampal sharp waves: their origin and significance. Brain Res. 1986; 398:242–252. [PubMed: 3026567]

Buzsaki G. Two-stage model of memory trace formation: a role for "noisy" brain states. Neuroscience. 1989; 31:551–570. [PubMed: 2687720]

Buzsaki G. The hippocampo-neocortical dialogue. Cereb Cortex. 1996; 6:81–92. [PubMed: 8670641]

Buzsaki G. Hippocampal sharp wave-ripple: A cognitive biomarker for episodic memory and planning. Hippocampus. 2015; 25:1073–1188. [PubMed: 26135716]

Buzsaki G, Buhl DL, Harris KD, Csicsvari J, Czeh B, Morozov A. Hippocampal network patterns of activity in the mouse. Neuroscience. 2003; 116:201–211. [PubMed: 12535953]

Buzsaki G, Horvath Z, Urioste R, Hetke J, Wise K. High-frequency network oscillation in the hippocampus. Science. 1992; 256:1025–1027. [PubMed: 1589772]

Carr MF, Karlsson MP, Frank LM. Transient slow gamma synchrony underlies hippocampal memory replay. Neuron. 2012; 75:700–713. [PubMed: 22920260]

Cheng S, Frank LM. New experiences enhance coordinated neural activity in the hippocampus. Neuron. 2008; 57:303–313. [PubMed: 18215626]

Ciupek SM, Cheng J, Ali YO, Lu HC, Ji D. Progressive functional impairments of hippocampal neurons in a tauopathy mouse model. J Neurosci. 2015; 35:8118–8131. [PubMed: 26019329]

Clemens Z, Molle M, Eross L, Barsi P, Halasz P, Born J. Temporal coupling of parahippocampal ripples, sleep spindles and slow oscillations in humans. Brain. 2007; 130:2868–2878. [PubMed: 17615093]

Colgin LL. Slow gamma takes the reins in replay. Neuron. 2012; 75:549–550. [PubMed: 22920247]

Colgin LL, Denninger T, Fyhn M, Hafting T, Bonnevie T, Jensen O, Moser MB, Moser EI. Frequency of gamma oscillations routes flow of information in the hippocampus. Nature. 2009; 462:353–357. [PubMed: 19924214]

Corder EH, Saunders AM, Strittmatter WJ, Schmechel DE, Gaskell PC, Small GW, Roses AD, Haines JL, Pericak-Vance MA. Gene dose of apolipoprotein E type 4 allele and the risk of Alzheimer's disease in late onset families. Science. 1993; 261:921–923. [PubMed: 8346443]

Csicsvari J, Hirase H, Mamiya A, Buzsaki G. Ensemble patterns of hippocampal CA3-CA1 neurons during sharp wave-associated population events. Neuron. 2000; 28:585–594. [PubMed: 11144366]

Csicsvari J, Jamieson B, Wise KD, Buzsaki G. Mechanisms of gamma oscillations in the hippocampus of the behaving rat. Neuron. 2003; 37:311–322. [PubMed: 12546825]

Ego-Stengel V, Wilson MA. Disruption of ripple-associated hippocampal activity during rest impairs spatial learning in the rat. Hippocampus. 2010; 20:1–10. [PubMed: 19816984]

Farrer LA, Cupples LA, Haines JL, Hyman B, Kukull WA, Mayeux R, Myers RH, Pericak-Vance MA, Risch N, van Duijn CM. Effects of age, sex, and ethnicity on the association between apolipoprotein E genotype and Alzheimer disease. A meta-analysis APOE and Alzheimer Disease Meta Analysis Consortium. JAMA. 1997; 278:1349–1356. [PubMed: 9343467]

Girardeau G, Benchenane K, Wiener SI, Buzsaki G, Zugaro MB. Selective suppression of hippocampal ripples impairs spatial memory. Nat Neurosci. 2009; 12:1222–1223. [PubMed: 19749750]

Huang Y, Mucke L. Alzheimer mechanisms and therapeutic strategies. Cell. 2012; 148:1204–1222. [PubMed: 22424230]

Jadhav SP, Kemere C, German PW, Frank LM. Awake hippocampal sharp-wave ripples support spatial memory. Science. 2012; 336:1454–1458. [PubMed: 22555434]

Karlsson MP, Frank LM. Network dynamics underlying the formation of sparse, informative representations in the hippocampus. J Neurosci. 2008; 28:14271–14281. [PubMed: 19109508]

Knoferle J, Yoon SY, Walker D, Leung L, Gillespie AK, Tong LM, Bien-Ly N, Huang Y. Apolipoprotein E4 produced in GABAergic interneurons causes learning and memory deficits in mice. J Neurosci. 2014; 34:14069–14078. [PubMed: 25319703]

Kudrimoti HS, Barnes CA, McNaughton BL. Reactivation of hippocampal cell assemblies: effects of behavioral state, experience, and EEG dynamics. J Neurosci. 1999; 19:4090–4101. [PubMed: 10234037]

Larkin MC, Lykken C, Tye LD, Wickelgren JG, Frank LM. Hippocampal output area CA1 broadcasts a generalized novelty signal during an object-place recognition task. Hippocampus. 2014; 24:773–783. [PubMed: 24596296]

Le Van Quyen M, Bragin A, Staba R, Crepon B, Wilson CL, Engel J Jr. Cell type-specific firing during ripple oscillations in the hippocampal formation of humans. J Neurosci. 2008; 28:6104–6110. [PubMed: 18550752]

Lee AK, Wilson MA. Memory of sequential experience in the hippocampus during slow wave sleep. Neuron. 2002; 36:1183–1194. [PubMed: 12495631]

Lega B, Burke J, Jacobs J, Kahana MJ. Slow-Theta-to-Gamma Phase-Amplitude Coupling in Human Hippocampus Supports the Formation of New Episodic Memories. Cereb Cortex. 2016; 26:268–278. [PubMed: 25316340]

Leung L, Andrews-Zwilling Y, Yoon SY, Jain S, Ring K, Dai J, Wang MM, Tong L, Walker D, Huang Y. Apolipoprotein E4 causes age- and sex-dependent impairments of hilar GABAergic interneurons and learning and memory deficits in mice. PLoS ONE. 2012; 7:e53569. [PubMed: 23300939]

Mann EO, Paulsen O. Mechanisms underlying gamma ('40 Hz') network oscillations in the hippocampus--a mini-review. Prog Biophys Mol Biol. 2005; 87:67–76. [PubMed: 15471591]

Montgomery SM, Buzsaki G. Gamma oscillations dynamically couple hippocampal CA3 and CA1 regions during memory task performance. Proc Natl Acad Sci USA. 2007; 104:14495–14500. [PubMed: 17726109]

Myers CE, Scharfman HE. Pattern separation in the dentate gyrus: a role for the CA3 backprojection. Hippocampus. 2011; 21:1190–1215. [PubMed: 20683841]

Nakashiba T, Buhl DL, McHugh TJ, Tonegawa S. Hippocampal CA3 output is crucial for ripple-associated reactivation and consolidation of memory. Neuron. 2009; 62:781–787. [PubMed: 19555647]

O'Neill J, Senior TJ, Allen K, Huxter JR, Csicsvari J. Reactivation of experience-dependent cell assembly patterns in the hippocampus. Nat Neurosci. 2008; 11:209–215. [PubMed: 18193040]

Penttonen M, Kamondi A, Sik A, Acsady L, Buzsaki G. Feed-forward and feed-back activation of the dentate gyrus in vivo during dentate spikes and sharp wave bursts. Hippocampus. 1997; 7:437–450. [PubMed: 9287083]

Pfeiffer BE, Foster DJ. Hippocampal place-cell sequences depict future paths to remembered goals. Nature. 2013; 497:74–79. [PubMed: 23594744]

Pfeiffer BE, Foster DJ. Autoassociative dynamics in the generation of sequences of hippocampal place cells. Science. 2015; 349:180–183. [PubMed: 26160946]

Potter GB, Petryniak MA, Shevchenko E, McKinsey GL, Ekker M, Rubenstein JL. Generation of Cre-transgenic mice using Dlx1/Dlx2 enhancers and their characterization in GABAergic interneurons. Mol Cell Neurosci. 2009; 40:167–186. [PubMed: 19026749]

Ramaswamy G, Xu Q, Huang Y, Weisgraber KH. Effect of domain interaction on apolipoprotein E levels in mouse brain. J Neurosci. 2005; 25:10658–10663. [PubMed: 16291938]

Ramsden M, Kotilinek L, Forster C, Paulson J, McGowan E, SantaCruz K, Guimaraes A, Yue M, Lewis J, Carlson G, Hutton M, Ashe KH. Age-dependent neurofibrillary tangle formation, neuron loss, and memory impairment in a mouse model of human tauopathy (P301L). J Neurosci. 2005; 25:10637–10647. [PubMed: 16291936]

Santacruz K, Lewis J, Spires T, Paulson J, Kotilinek L, Ingelsson M, Guimaraes A, DeTure M, Ramsden M, McGowan E, Forster C, Yue M, Orne J, Janus C, Mariash A, Kuskowski M, Hyman B, Hutton M, Ashe KH. Tau suppression in a neurodegenerative mouse model improves memory function. Science. 2005; 309:476–481. [PubMed: 16020737]

Saunders AM, Strittmatter WJ, Schmechel D, George-Hyslop PH, Pericak-Vance MA, Joo SH, Rosi BL, Gusella JF, Crapper-MacLachlan DR, Alberts MJ. Association of apolipoprotein E allele epsilon 4 with late-onset familial and sporadic Alzheimer's disease. Neurology. 1993; 43:1467–1472. [PubMed: 8350998]

Scharfman HE. The CA3 "backprojection" to the dentate gyrus. Prog Brain Res. 2007; 163:627–637. [PubMed: 17765742]

Sederberg PB, Schulze-Bonhage A, Madsen JR, Bromfield EB, Litt B, Brandt A, Kahana MJ. Gamma oscillations distinguish true from false memories. Psychol Sci. 2007; 18:927–932. [PubMed: 17958703]

Skaggs WE, McNaughton BL. Replay of neuronal firing sequences in rat hippocampus during sleep following spatial experience. Science. 1996; 271:1870–1873. [PubMed: 8596957]

Strittmatter WJ, Saunders AM, Schmechel D, Pericak-Vance M, Enghild J, Salvesen GS, Roses AD. Apolipoprotein E: high-avidity binding to beta-amyloid and increased frequency of type 4 allele in late-onset familial Alzheimer disease. Proc Natl Acad Sci USA. 1993; 90:1977–1981. [PubMed: 8446617]

Sullivan D, Csicsvari J, Mizuseki K, Montgomery S, Diba K, Buzsaki G. Relationships between hippocampal sharp waves, ripples, and fast gamma oscillation: influence of dentate and entorhinal cortical activity. J Neurosci. 2011; 31:8605–8616. [PubMed: 21653864]

Sullivan PM, Mace BE, Maeda N, Schmechel DE. Marked regional differences of brain human apolipoprotein E expression in targeted replacement mice. Neuroscience. 2004; 124:725–733. [PubMed: 15026113]

Tong LM, Djukic B, Arnold C, Gillespie AK, Yoon SY, Wang MM, Zhang O, Knoferle J, Rubenstein JLR, Alvarez-Buylla A, Huang Y. Inhibitory interneuron progenitor transplantation restores normal learning and memory in apoE4-KI mice without or with Aβ accumulation. J Neurosci. 2014; 34:9506–9515. [PubMed: 25031394]

Witton J, Staniaszek LE, Bartsch U, Randall AD, Jones MW, Brown JT. Disrupted hippocampal sharp-wave ripple-associated spike dynamics in a transgenic mouse model of dementia. J Physiol. 2014 in press.

Ylinen A, Bragin A, Nadasdy Z, Jando G, Szabo I, Sik A, Buzsaki G. Sharp wave-associated high-frequency oscillation (200 Hz) in the intact hippocampus: network and intracellular mechanisms. J Neurosci. 1995; 15:30–46. [PubMed: 7823136]
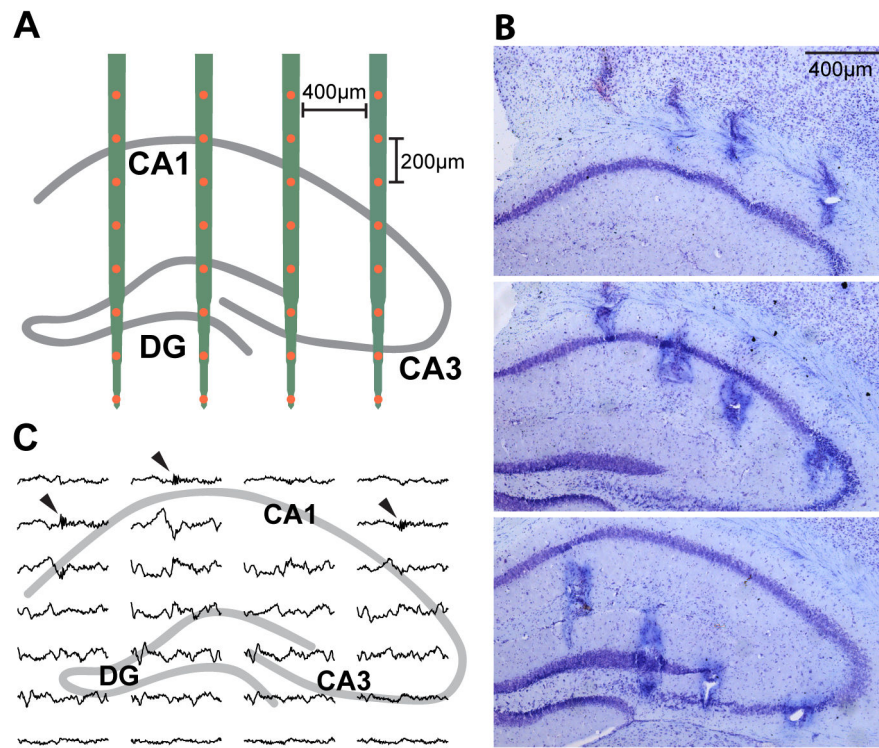
Figure 1. LFP recording of hippocampal network activity in apoE3-KI and apoE4-KI mice

(A) Schematic representation of probe placement in the dorsal hippocampus, targeting CA1, CA3, and the DG.

(B) Representative Nissl staining of brain sections after electrolytic lesioning indicates probe placement, shown in sequential coronal sections.

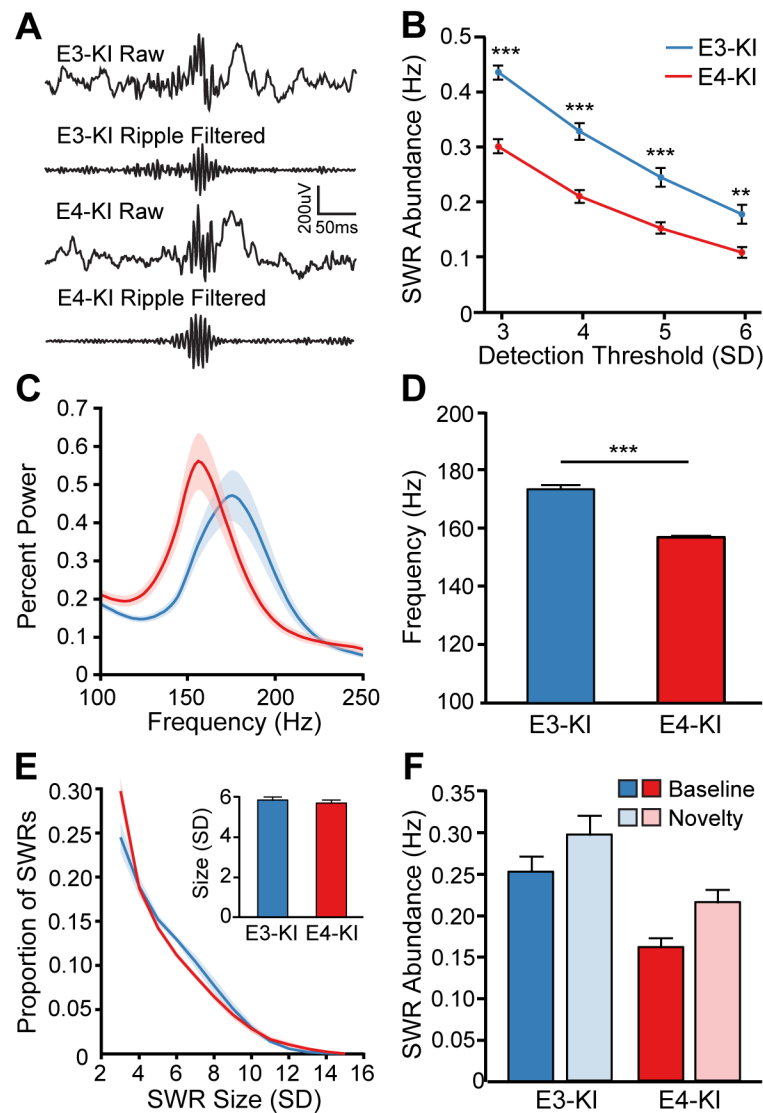(C) Sample data (800 ms) shown across all recording sites. Arrowheads indicate SWRs in CA1 pyramidal cell layer sites.

Figure 2. SWR abundance is reduced in aged apoE4-KI mice

(A) Representative raw traces and filtered ripple band traces (150–250 Hz) from aged apoE3-KI and apoE4-KI mice.

(B) The abundance of SWRs detected with thresholds of 3, 4, 5, and 6 SD above baseline (unpaired t tests; t(25) = 7.302, 6.193, 4.565, and 3.488, respectively).

(C) Percent power spectra of aged apoE3-KI and apoE4-KI mice during SWRs.

(D) Frequency of peak ripple power in aged apoE3-KI and apoE4-KI mice (unpaired t test; t(25) = 10.34).

(E) Distribution of SWR sizes (in units of SD). Inset: Average ripple size (in SD).

(F) SWR abundance after exposure to novel environments, 5 SD threshold. Two-way ANOVA shows significant effect of genotype ($P < 0.001$, F(1,50) = 23.88) and environment ($P < 0.01$, F(1,50) = 7.421), but no interaction between them.

**$P < 0.01$; ***$P < 0.001$. n = 14 and 13 for aged apoE3-KI and apoE4-KI groups, respectively. Error bars and shading indicate SEM. See also Figure S1.
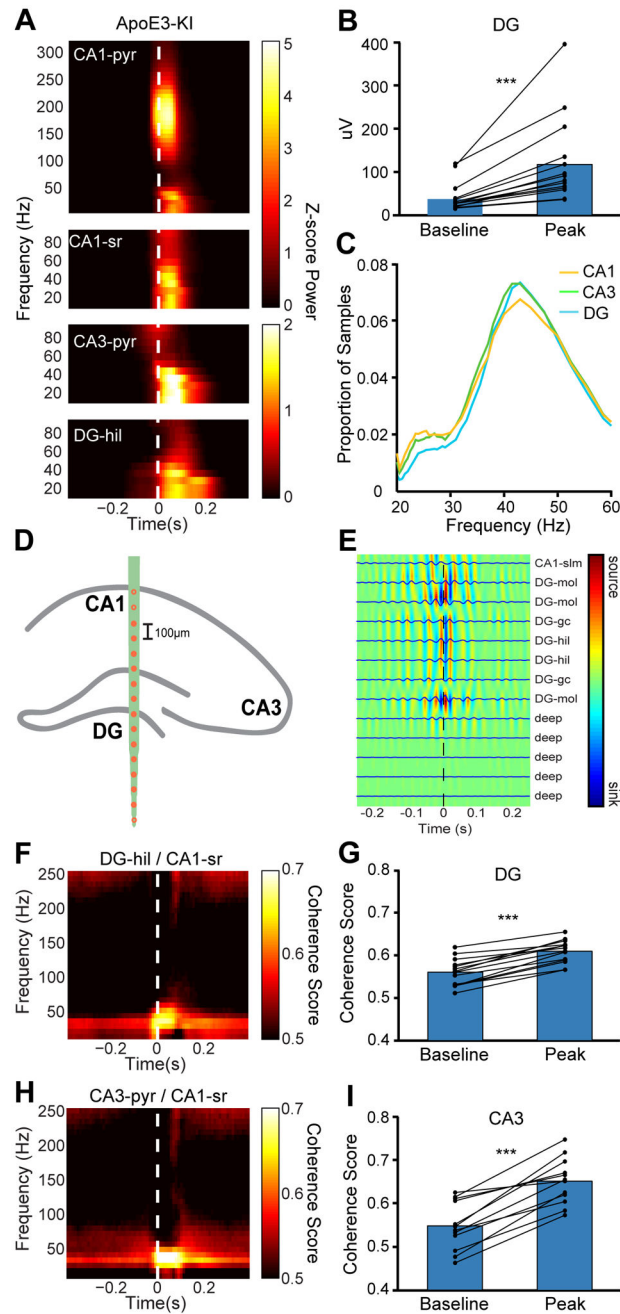
Figure 3. Transient slow gamma oscillation during SWRs in CA1, CA3, and DG of the hippocampus in apoE3-KI mice

(A) Representative examples of SWR-triggered spectrograms from CA1 pyramidal cell layer (CA1-pyr), CA1 stratum radiatum (CA1-sr), CA3 pyramidal cell layer (CA3-pyr), and DG hilus (DG-hil) in an apoE3-KI mouse. White dashed line represents threshold crossing for SWR detection.

(B) Average increase in slow gamma power from baseline (350 ms before SWR detection) to peak of SWR in DG for all apoE3-KI mice (paired *t* test; t(13) = 4.348, *n* = 14).

(C) Distribution of instantaneous frequency measurements in all three hippocampal subregions.

(D) Schematic representation of site location in an apoE3-KI mouse receiving a probe with 100-μm site spacing. Filled circles indicate sites used for CSD analysis.

(E) SWR-triggered CSD profile indicates distinct regions of slow gamma activity in DG region. Color and traces represent averaged (traces) and smoothed (color) CSD values based on LFP signal filtered for slow gamma activity (30–50 Hz), averaged across SWRs. Note phase reversal across granule cell layers, indicating local origin of activity. Sites include CA1 stratum lacunosum-moleculare (CA1-slm), DG molecular layer (DG-mol), DG granule cell layer (DG-gc), and DG hilus (DG-hil). Deep sites are located outside the hippocampal formation.

(F) SWR-triggered coherogram between DG hilus and CA1 stratum radiatum.

(G) Quantification of coherence between DG and CA1 stratum radiatum at baseline (400–300 ms before SWR detection) and SWR peak (0–100 ms after SWR detection) for all apoE3-KI mice (paired t test; t(13) = 10.86, n = 14).

(H) SWR-triggered coherogram between CA3 pyramidal cell layer and CA1 stratum radiatum.

(I) Quantification of coherence between CA3 and CA1 stratum radiatum at baseline (400–300 ms before SWR detection) and SWR peak (0–100 ms after SWR detection) for all apoE3-KI mice (paired t test; t(13) = 8.082, n = 14).
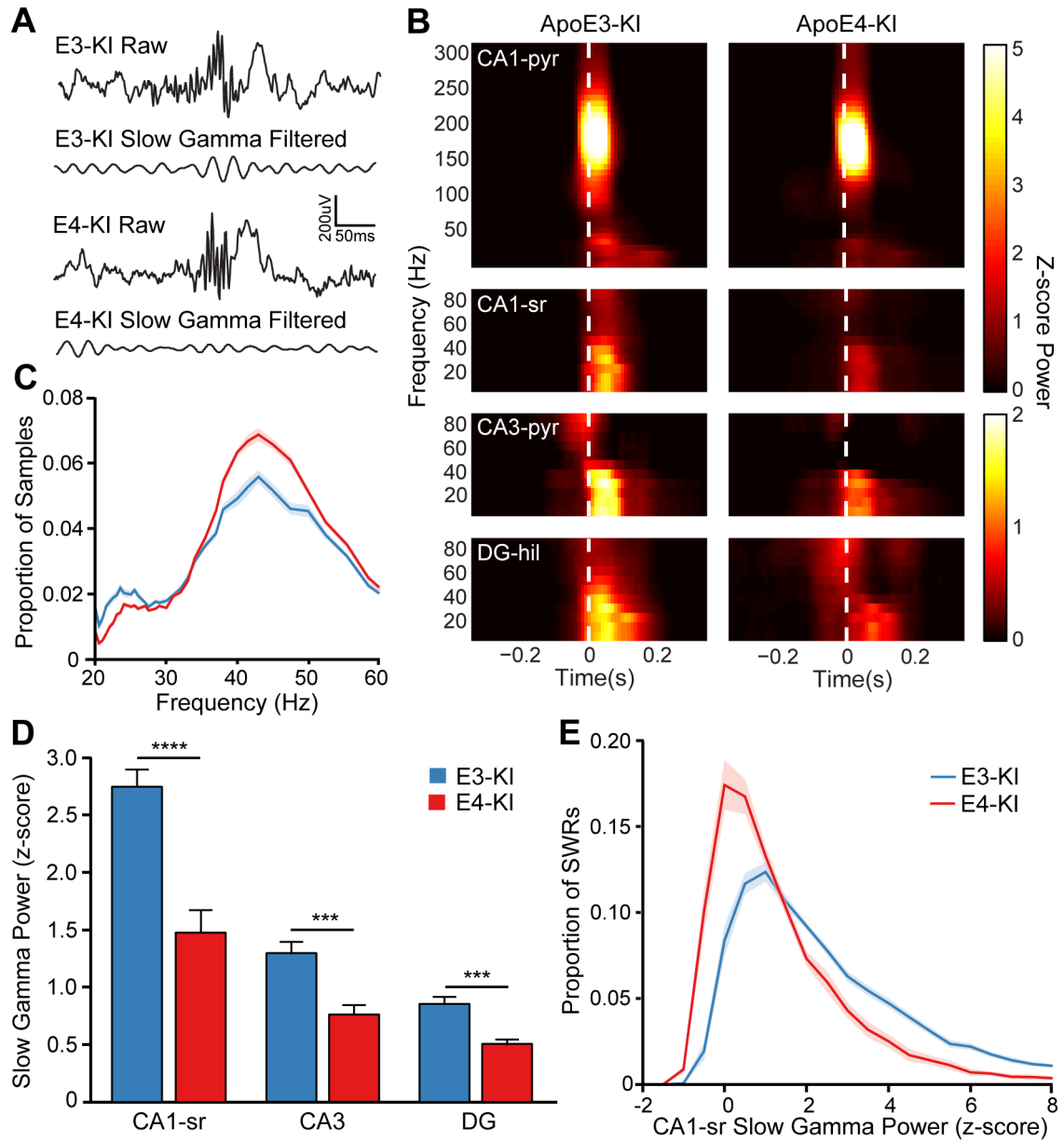
***P < 0.001. See also Figure S2

Figure 4. SWR-associated slow gamma power is reduced in aged apoE4-KI mice

(A) Raw and slow gamma filtered traces (30–50 Hz) surrounding a representative SWR (same SWR as in Figure 2) in aged apoE3-KI and apoE4-KI mice.

(B) SWR-triggered spectrograms from representative aged apoE3-KI and apoE4-KI mice from CA1 pyramidal cell layer (CA1-pyr), CA1 stratum radiatum (CA1-sr), CA3 pyramidal cell layer (CA3-pyr), and DG hilus (DG-hil). White dashed line represents threshold crossing for SWR detection.

(C) Distribution of instantaneous frequency measurements of slow gamma in CA1-sr of aged apoE3-KI and apoE4-KI mice.

(D) Quantification of z-scored slow gamma power during SWRs in CA1-sr, CA3, and DG (unpaired *t* test; t(25) = 5.236 and 4.896 for CA1-sr and DG, respectively; *n* = 14 and 13 for

apoE3-KI and apoE4-KI groups, respectively. t(21) = 4.093 for CA3; n = 12 and 11, for apoE3-KI and apoE4-KI groups, respectively).

(E) Distribution of SWR-associated slow gamma power (z-scored) in CA1-sr across all SWRs in aged apoE3-KI and apoE4-KI mice.

***P< 0.001; ****P< 0.0001. Error bars and shading indicate SEM. See also Figure S3 and S4.
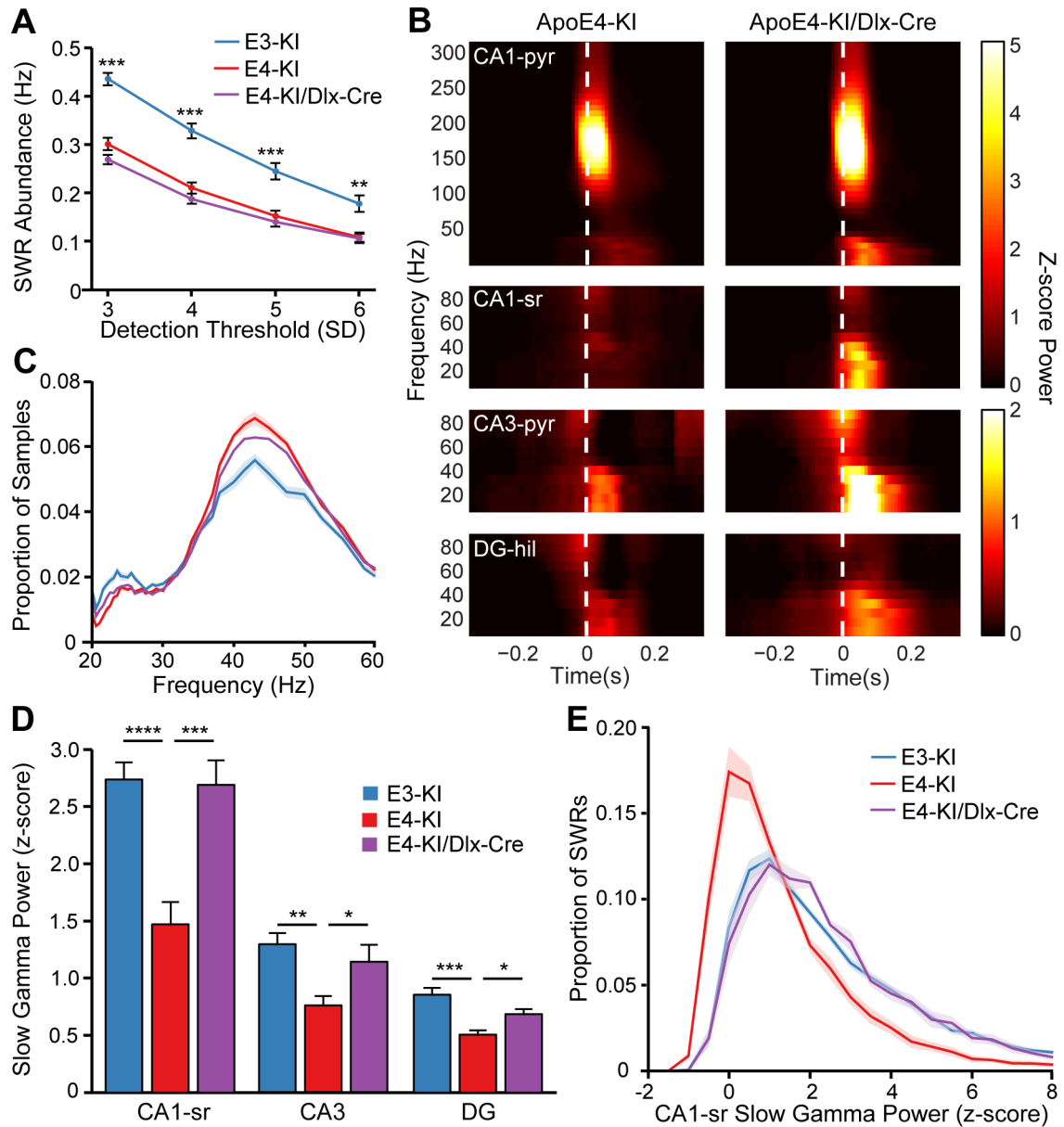
Figure 5. Removal of apoE4 from GABAergic interneurons rescues SWR-associated slow gamma power but not SWR abundance

(A) SWR abundance at various thresholds. Significance indicated in respect to apoE4-KI group (one-way ANOVA with corrected post-hoc tests; $F_{(2,32)}$ = 47.2, 32.59, 17.02, 9.265).

(B) Representative SWR-triggered spectrograms from CA1 pyramidal cell layer (CA1-pyr), CA1 stratum radiatum (CA1-sr), CA3 pyramidal cell layer (CA3-pyr), and DG hilus (DG-hil) of aged apoE4-KI and apoE4-KI/Dlx-Cre mice. White dashed line represents threshold crossing for SWR detection.

(C) Distribution of instantaneous frequency measurements in CA1-sr.

(D) Quantification of SWR-associated slow gamma power (z-scored) in hippocampal subregions (for CA1-sr, CA3, and DG, one-way ANOVA with corrected post-hoc tests; $F_{(2,32)}$ = 16.16, 7.701, 13.65 respectively).

(E) Distribution of SWR-associated slow gamma power (z-scored) in CA1-sr.

*$P < 0.05$; **$P < 0.01$; ***$P < 0.001$; ****$P < 0.0001$. $n = 14$, 13, and 8 for apoE3-KI, apoE4-KI, and apoE4/Dlx-Cre groups, respectively, except in CA3 subregion, where $n = 12$, 11, and 8, respectively. Error bars and shading indicate SEM. See also Figure S5.
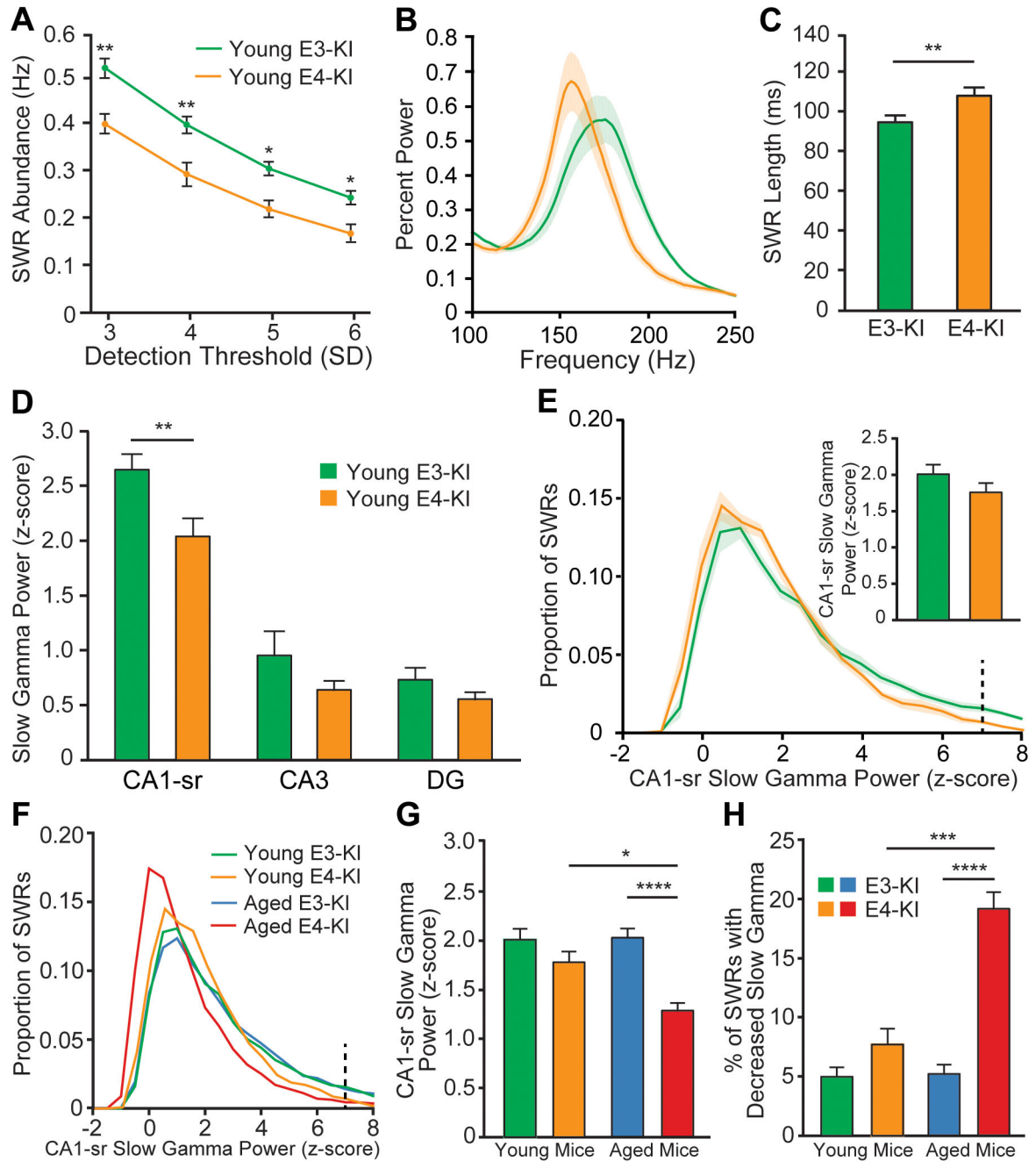
Figure 6. SWR and SWR-associated slow gamma characteristics in young apoE3-KI and apoE4-KI mice are differentially affected by aging

(A) SWR abundance in 4–5-month-old apoE3-KI and apoE4-KI mice at 3, 4, 5, and 6 SD thresholds. (unpaired *t* tests; t(14) = 3.129, 3.126, 2.939, and 2.634, respectively).

(B) Percent power spectra during SWRs. Frequency of peak ripple power is significantly lower in young apoE4-KI mice than in young apoE3-KI mice; 156.0 ± 1.562 Hz vs 175.1 ± 1.98 Hz, (unpaired *t* test, *P* < 0.0001; t(14) = 7.252).

(C) Quantification of average SWR length in young apoE3-KI and young apoE4-KI mice (unpaired t-test, t(14) = 3.431)

(D) Quantification of SWR-associated slow gamma power (z-scored) in hippocampal subregions (unpaired t test; t(14) = 3.281 for CA1-sr).

(E) Distribution of SWR-associated slow gamma power (z-scored) in CA1-sr. Inset: Recalculation of average SWR-associated slow gamma power excluding events with z-scored slow gamma power > 7 (dashed line).

(F) Distribution of SWR-associated slow gamma power (z-scored) in CA1-sr for all genotype and age groups.

(G) SWR-associated slow gamma power in CA1 stratum radiatum recalculated after exclusion of events with z-scored slow gamma power > 7 (dashed line in panel F). Two-way ANOVA with corrected post-hoc tests shows significant effects of genotype ($P < 0.0001$, F(1,39) = 23.00) and age ($P = 0.0388$, F(1,39) =4.571) and significant interaction between the two ($P = 0.0263$, F(1,39) = 5.332).

(H) Fraction of SWRs with suppressed CA1 stratum radiatum slow gamma activity below baseline (z-score power < 0) for all genotype and age groups. Two way ANOVA with corrected post-hoc tests shows significant effects of genotype ($P < 0.0001$, F(1,39) = 32.84) and age ($P = 0.0013$, F(1,39) = 11.92) and significant interaction between the two ($P = 0.0033$, F(1,39) = 9.823).

*$P < 0.05$; **$P < 0.01$; ***$P < 0.001$; ****$P < 0.0001$. $n = 9$ and 7 for young apoE3-KI and apoE4-KI, respectively; $n = 14$ and 13 for aged apoE3-KI and apoE4-KI, respectively. Error bars and shading indicate SEM. See also Figure S6.
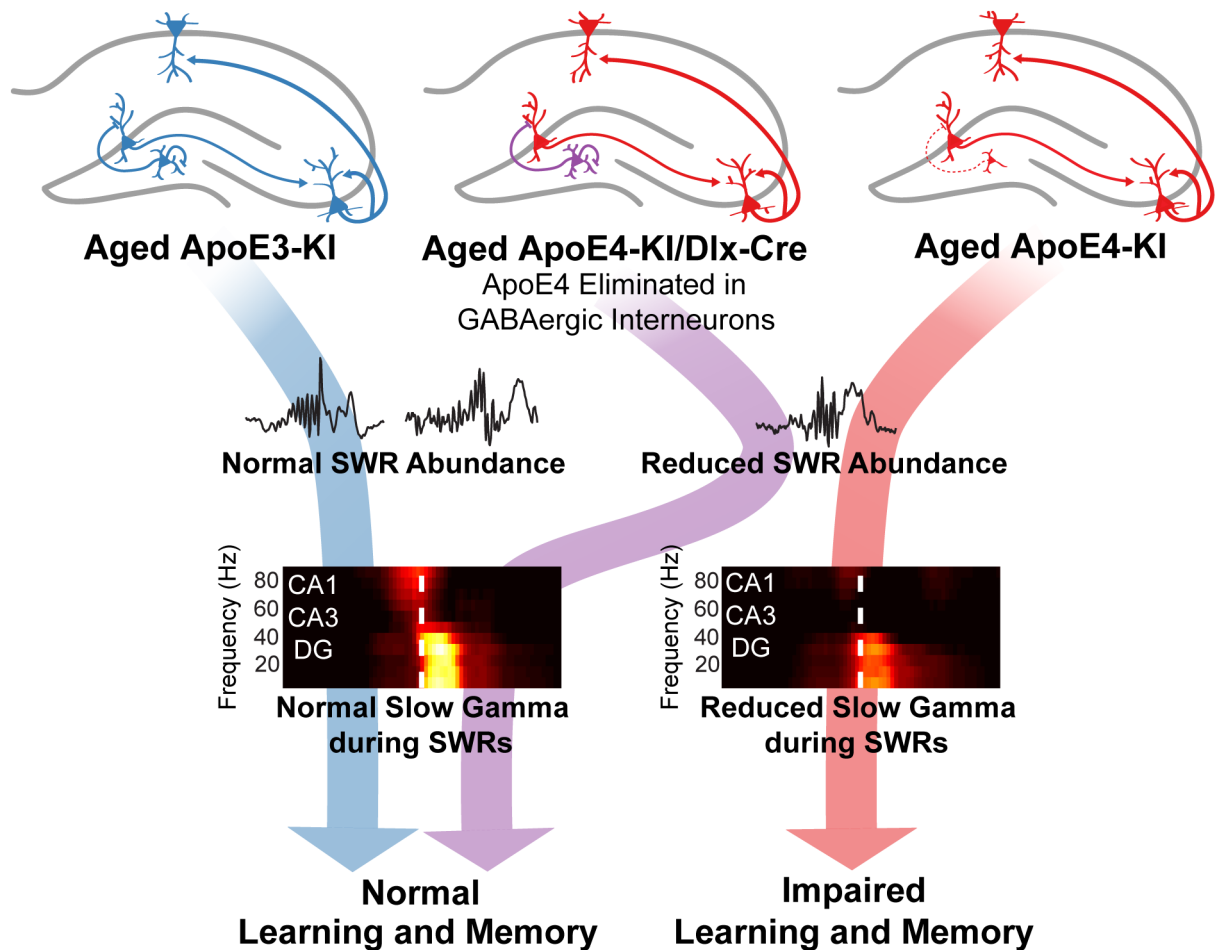
Figure 7. Deficit in DG-enabled slow gamma oscillations during SWRs likely contributes to apoE4-induced learning and memory impairments in aged mice

Compared to aged apoE3-KI mice, aged apoE4-KI mice show significant loss of GABAergic interneurons in the hilus of the DG. This loss is prevented by removing apoE4 from GABAergic interneurons, as seen in aged apoE4-KI/Dlx-Cre mice. Aged ApoE4-KI and apoE4-KI/Dlx-Cre mice have fewer SWRs than aged apoE3-KI mice. Transient slow gamma activity occurs in the CA1, CA3, and DG during SWRs and is attenuated in throughout the hippocampal circuit in aged apoE4-KI mice. Strikingly, in aged apoE4-KI/Dlx-Cre mice, which do not develop learning and memory impairments (Knoferle et al., 2014), SWR-associated slow gamma power is restored to the level as in aged apoE3-KI mice. Together, these findings suggest that progressive dysregulation of SWR-associated slow gamma activity contributes to age-dependent learning and memory impairment in apoE4-KI mice.